

# Optical Engineering

OpticalEngineering.SPIEDigitalLibrary.org

## Astigmatic Herriott cell for optical refrigeration

Aram Gragossian  
Junwei Meng  
Mohammadreza Ghasemkhani  
Alexander R. Albrecht  
Mansoor Sheik-Bahae

**SPIE.**

Aram Gragossian, Junwei Meng, Mohammadreza Ghasemkhani, Alexander R. Albrecht, Mansoor Sheik-Bahae, "Astigmatic Herriott cell for optical refrigeration," *Opt. Eng.* **56**(1), 011110 (2016), doi: 10.1117/1.OE.56.1.011110.

# Astigmatic Herriott cell for optical refrigeration

Aram Gragossian, Junwei Meng, Mohammadreza Ghasemkhani, Alexander R. Albrecht, and Mansoor Sheik-Bahae\*  
University of New Mexico, Department of Physics and Astronomy, 1919 Lomas Boulevard Northeast, Albuquerque, New Mexico 87131, United States

**Abstract.** Cooling rare-earth-doped crystals to the lowest temperature possible requires enhanced resonant absorption and high-purity crystals. Since resonant absorption decreases as the crystal is cooled, the only path forward is to increase the number of roundtrips that the laser makes inside the crystal. To achieve even lower temperatures than previously reported, we have employed an astigmatic Herriott cell to improve laser absorption at low temperatures. Preliminary results indicate improvement over previous designs. This cavity potentially enables us to use unpolarized high-power fiber lasers, and to achieve much higher cooling power for practical applications. © 2016 Society of Photo-Optical Instrumentation Engineers (SPIE) [DOI: 10.1117/1.OE.56.1.011110]

Keywords: optical refrigeration; laser cooling of solids; Herriott cell.

Paper 161299SS received Aug. 18, 2016; accepted for publication Nov. 2, 2016; published online Dec. 16, 2016.

The resonant absorption originating from the top of the ground state in rare-earth ions (as in E4–E5 transition in Yb<sup>3+</sup>) sharply drops as the lattice temperature drops due to the Boltzmann distribution of populations in that manifold. From a four-level model, it approximately scales as  $\sim [1 + \exp(\delta E_g/k_B T)]^{-1}$ , where  $\delta E_g$  is the width of the ground-state manifold.<sup>1,2</sup> For a 5% doped Yb:YLF crystal ( $\delta E_g \approx 460 \text{ cm}^{-1}$ ), the absorption coefficient  $\alpha_r$  versus the lattice temperature at the optimum cooling wavelength of  $\lambda = 1020 \text{ nm}$  (E4–E5 transition) is shown in Fig. 1. The laser coupling efficiency  $\eta_{\text{cpl}}$ , defined as the fraction of the incident laser power ( $P_{\text{in}}$ ) that is absorbed in the cooling crystal (ignoring the parasitic losses), is

$$\eta_{\text{cpl}} = \frac{P_{\text{abs}}}{P_{\text{in}}} = 1 - \exp(-2N_{\text{rt}}\alpha_r L_c), \quad (1)$$

where  $N_{\text{rt}}$  is the number of roundtrips that the laser makes through the crystal. Assuring  $\eta_{\text{cpl}} > 95\%$  requires  $N_{\text{rt}}\alpha_r L_c > 1.5$ . For a typical  $L_c = 1\text{-cm}$  long crystal, this in turn demands (from Fig. 1) that we provide  $N_{\text{rt}} > 150$  for  $T = 100 \text{ K}$ , and  $N_{\text{rt}} > 60$  for  $T = 120 \text{ K}$ .

While resonant cavity<sup>3</sup> as well as laser intracavity<sup>4,5</sup> geometries have been exploited, and have exhibited certain advantages, the nonresonant multipass cavities (Herriott cells) offer a simple and practical solution that can produce very high coupling efficiency. Here, we analyze the utility of an astigmatic Herriott cell for optical refrigeration. We further introduce a geometry that can accommodate unpolarized laser light with high coupling efficiency into a Brewster-cut sample. In our analysis, we have in mind a typical rare earth-doped crystal (e.g., Yb-doped YLF), and linearly polarized laser light ( $E \parallel c$  for maximum absorption), and to minimize Fresnel losses by utilizing a Brewster-cut geometry as shown in Fig. 2, for a crystal with a square cross section ( $W_x = W_y = W$ ).

Astigmatic cells of the type shown here have been analyzed by Herriott and Schulte,<sup>6</sup> and later further analyzed by McManus et al.<sup>7</sup> The laser is launched into the crystal through a small hole at the center of the mirror 1 and makes many roundtrips between this mirror and mirror 2 each having toroidal surfaces with radii of curvature  $R_{1,x,y}$  and  $R_{2,x,y}$ . From the ABCD matrix approach under paraxial approximation, it can be shown that the position ( $X_m$  and  $Y_m$ ) of the light ray on mirror 1 after  $m$ 'th roundtrip is as follows:

$$\begin{pmatrix} X_m \\ Y_m \end{pmatrix} = \begin{bmatrix} X_{\text{max}} \sin(m\theta_x) \\ Y_{\text{max}} \sin(m\theta_y) \end{bmatrix}, \quad (2)$$

where  $\theta_j = \sin^{-1}[2\sqrt{g_{1j}g_{2j}(1-g_{1j}g_{2j})}]$ , with  $g_{1j} = [1 - (L/R_{1j})]$  and  $g_{2j} = [1 - (L/R_{2j})]$  for  $j = x, y$ . Here, we define the effective length  $L = D + (1-n)L_c/n$ , where  $n$  is the refractive index of the crystal. The values for  $X_{\text{max}}$  and  $Y_{\text{max}}$ , which should be selected to be smaller than the transverse dimensions of the crystal, are controlled by the launching angles  $\Phi_{x,y}$  of the incident ray (laser beam) through the entrance hole. We find these to be

$$\begin{aligned} \Phi_x &= \frac{X_{\text{max}} \sqrt{g_{1x}g_{2x}(1-g_{1x}g_{2x})}}{L g_{2x}}, \\ \Phi_y &= \frac{Y_{\text{max}} \sqrt{g_{1y}g_{2y}(1-g_{1y}g_{2y})}}{L g_{2y}}. \end{aligned} \quad (3)$$

For practical cases where  $X_{\text{max}} = Y_{\text{max}} = W/2$ , and  $D \ll R$ 's, this simplifies to

$$\Phi_{x,y} \approx \frac{W}{2\sqrt{L\left(\frac{1}{R_{1,x,y}} + \frac{1}{R_{2,x,y}}\right)^{-1}}}. \quad (4)$$

The fidelity of such a cell is defined as the maximum number of roundtrips before the ray totally or partially exits through the entrance hole. McManus et al.<sup>7</sup> described such a figure of

\*Address all correspondence to: Mansoor Sheik-Bahae, E-mail: [msb@unm.edu](mailto:msb@unm.edu)

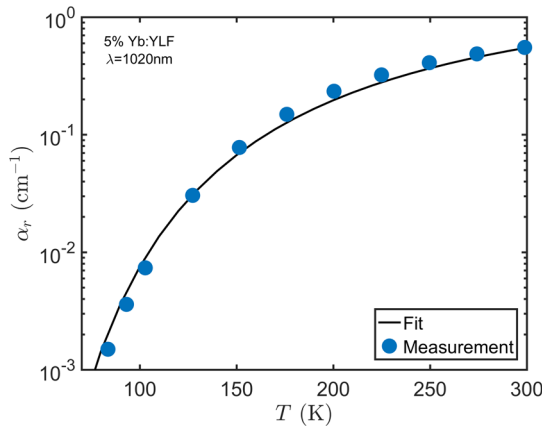


**Fig. 1** Measured absorption coefficient of 5% Yb:YLF (circles) at 1020 nm corresponding to E4-E5 transition between the Stark manifolds. The solid line follows  $\sim [1 + \exp(\delta E_g/k_B T)]^{-1}$ , where  $\delta E_g \sim 460 \text{ cm}^{-1}$  is the width of the ground-state manifold in this material.

merit as the maximum number of roundtrips  $N_{rt}$  before the ray enters a zone of radius  $R_{min}$  centered around the entrance hole. This quantity varies significantly as a function of  $g_{1,x,y}$  and  $g_{2,x,y}$ . For example, assuming two cylindrical mirrors ( $R_{1,x} = R_{2,y} = \infty$ ), and taking  $R_{min} = 0.1 W$ ,  $N_{rt}$  shows an intriguing (fractal-like) pattern when evaluated versus  $g_{1,y}$  and  $g_{2,x}$  as shown in Fig. 3. As shown,  $N_{rt} \approx 250$  can be obtained for this particular geometry. Reducing  $R_{min}$  to  $0.05 W$  can increase  $N_{rt}$  to  $\approx 1000$ . For fixed values of radii of curvature, the azimuthal rotation of mirrors as well as variation in mirror separation ( $D$ ) can be utilized to fine tune the cavity to accommodate a maximum number of roundtrips. Needless to say, the effects of diffraction and poor beam quality (as in diode lasers) impose further restrictions on the maximum attainable roundtrips.

To compare with the cavity parameters in our experiments, we analyze a cavity constructed by a spherical mirror ( $R_{1,x} = R_{1,y} = 50 \text{ cm}$ ) and a cylindrical mirror ( $R_{2,x} = \infty$ ,  $R_{2,y} = 50 \text{ cm}$ ).

Assuming  $L_c = 1.4 \text{ cm}$ , we plot (Fig. 4) the position of the ray at the first mirror for 100 roundtrips. Taking  $X_{max} = Y_{max} = 2.5 \text{ mm}$  ( $W = 5 \text{ mm}$ ), we find  $\Phi_x = 1.8 \text{ deg}$  and  $\Phi_y = 1.26 \text{ deg}$ . A circle of  $R_{min} = 0.5 \text{ mm}$  is also shown in Fig. 4(a) indicating that no re-entry (into this circle) occurs in  $>100$  bounces. Plotting  $R_m = (X_m^2 + Y_m^2)^{1/2}$  versus  $N$  [Fig. 4(b)] indicates that the beam barely enters in the

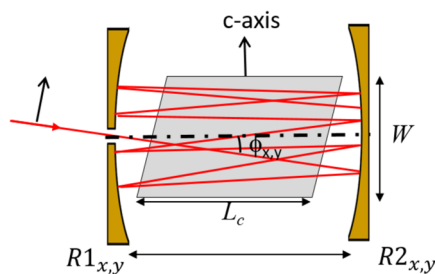


**Fig. 2** Schematic of a typical astigmatic Herriott cell where the light beam enters through a hole at the center of mirror 1 forming angles  $\Phi_{x,y}$  in the  $x-z$  and  $y-z$  planes, respectively. The polarization is often chosen as linear along the  $c$ -axis to maximize the absorption and also mitigate the Fresnel losses with Brewster-cut crystals.

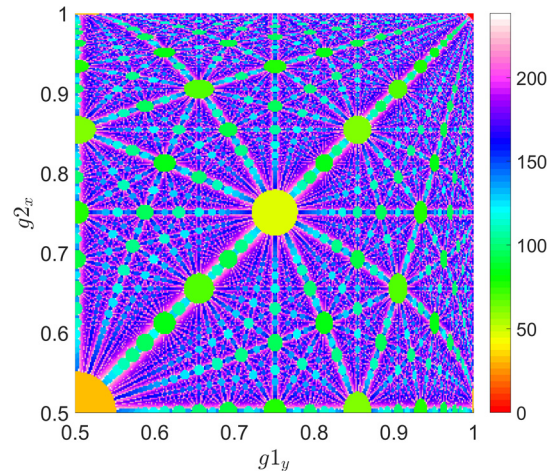
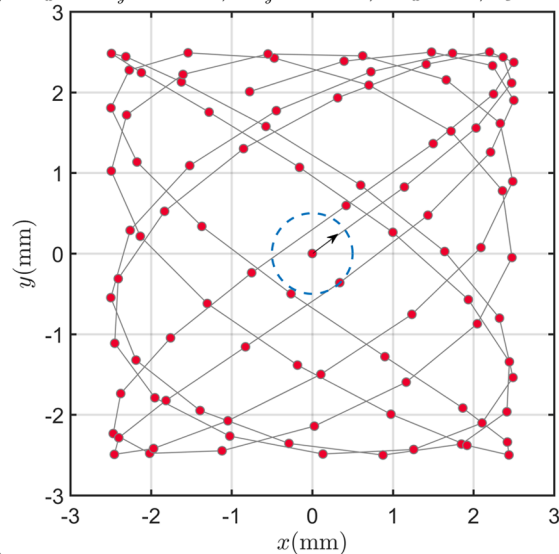


**Fig. 3** The number of roundtrips before re-entry into a zone of radius  $R_{min} = 0.1 W$  as a function of  $g$ -parameters of the cavity.

re-entry zone at the 96th roundtrip. With  $\alpha_r \approx 0.01 \text{ cm}^{-1}$  at a crystal temperature of  $100 \text{ K}$ , one obtains  $\eta_{cpl} > 90\%$  for  $L_c = 1.4 \text{ cm}$  and 100 roundtrips.

In the following, we examine the utility of the above analysis for solid-state laser cooling applications. First, we construct an astigmatic Herriott cell cavity similar to Fig. 1, using a spherical mirror ( $R = 50 \text{ cm}$ ) with a coupling

(a)  $R_{1,x} = R_{1,y} = 50 \text{ cm}$ ,  $R_{2,y} = 50 \text{ cm}$ ,  $R_{2,x} = \infty$ ,  $L_c = 1.4 \text{ cm}$



(b)

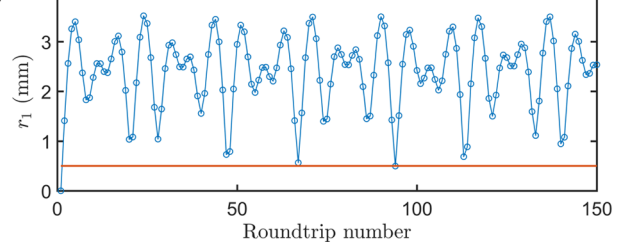


**Fig. 4** (a) Beam pattern and (b) the number of roundtrips before re-entry into a zone of radius  $R_{min} = 0.1 W$  as a function of  $g$ -parameters of the cavity. The beam would enter the  $R_{min}$  zone if the blue line crosses the red line. Size of the marker (circles) does not represent beam size.

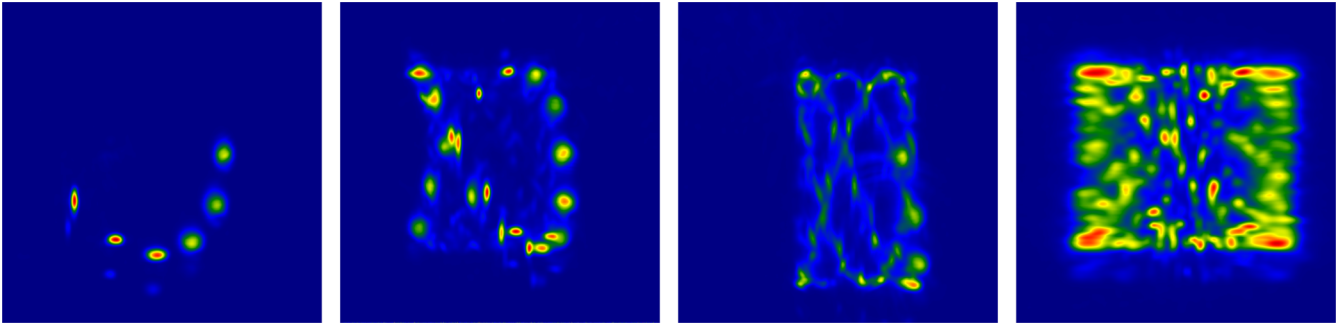


**Fig. 5** False-color plots of CCD camera images of light leaked through mirror 2 of the Herriott cell for (left to right) increasing number of passes achieved by improved alignment.

hole of 0.5-mm diameter at its center, and a cylindrical mirror having  $R_x = \infty$  (flat),  $R_y = 50$  cm (or vice versa). The cavity length ( $D$ ), without the cooling crystal is about 2.2 cm. We observe the light leaked through the second mirror using a CCD camera. The alignment is optimized by adjusting the tilt in both mirrors,  $\Phi_{x,y}$ , and cavity length, to maximize the number of laser spots, as shown in Fig. 5.

Second, to estimate the number of roundtrips inside the cavity, we insert a low-absorbing 3.2-mm thick sapphire window into the cavity at Brewster's angle to mimic a typical laser cooling arrangement. We use a thermal camera (Thermal Eye NanoCore Analog Infrared Camera 500655-1 w) to measure the temperature of the sample upon irradiation by a high-power laser (Yb-fiber) at  $\lambda = 1020$  nm. The temperature rise is measured in two arrangements: first, in the Herriott cell geometry, and second in a three-pass geometry, by replacing the spherical mirror with a semicircular flat mirror. We adjust the laser power so the amount of heating in both cases is nearly the same. Assuming the sapphire window has low absorption, the ratio of these two temperature changes (obtained from the thermal camera images) equals the ratio of the corresponding laser powers multiplied by the number of passes through the sapphire  $[(\Delta T_2/\Delta T_1) \approx (NP_2/3P_1)]$ . This yields an estimate of a minimum of 133 passes in the measured configuration.

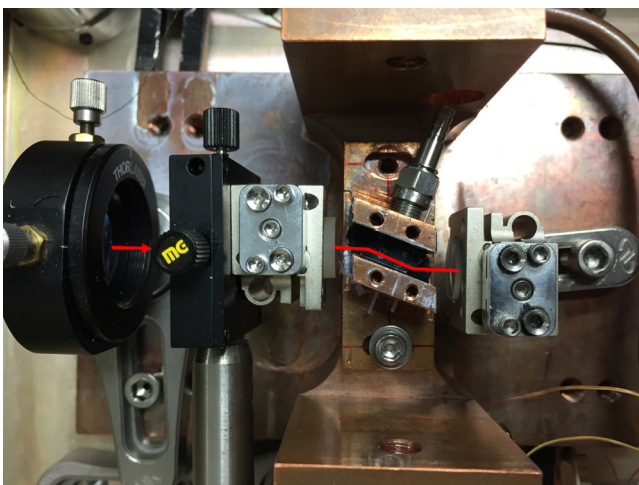


**Fig. 6** From left to right:  $f = 5$ -cm lens, spherical mirror ( $R = 50$  cm) with 0.5-mm hole at the center, crystal inside clamshell, and cylindrical mirror  $R_x = \infty$ ,  $R_y = 50$  cm.

Next, we present preliminary results of exploiting the above cavity in laser cooling of a 1.2-cm long Brewster-cut 5%Yb:YLF crystal. The experimental arrangement is shown in Fig. 6. The sample is placed in a tight-clamshell whose walls have high optical absorption but low thermal emissivity coating to minimize radiative thermal load.<sup>8</sup> The incident pump laser is a 50 W CW Yb-fiber laser ( $\lambda = 1020$  nm) that is coupled through the hole in mirror 1 using a 5-cm lens. The size of the beam at the entrance hole is measured to be  $157 \mu\text{m}$ .

The crystal temperature is measured by differential luminescence thermometry (DLT).<sup>9</sup> This noncontact method calculates the temperature by measuring the changes in the spectral shape of the normalized fluorescence

$$\Delta S(\lambda, T, T_0) = \frac{S(\lambda, T)}{\int_{\lambda_1}^{\lambda_2} S(\lambda, T) d\lambda} - \frac{S(\lambda, T_0)}{\int_{\lambda_1}^{\lambda_2} S(\lambda, T_0) d\lambda}, \quad (5)$$

where  $S$  is the spectral intensity and  $T_0$  is the initial temperature. Notice that the spectra are normalized to the area under the spectrum from  $\lambda_1$  to  $\lambda_2$ . This normalization minimizes any errors due to power fluctuation or collection efficiency. More importantly, since fluorescence is partially reabsorbed before it escapes the crystal,  $\lambda_1$  and  $\lambda_2$  must be in a range where spectral modulation is minimal. This is especially important for Herriott cells where fluorescence from multiple passes propagates through various depths. Once  $\lambda_1$  and  $\lambda_2$  are chosen, the DLT signal can be calculated by

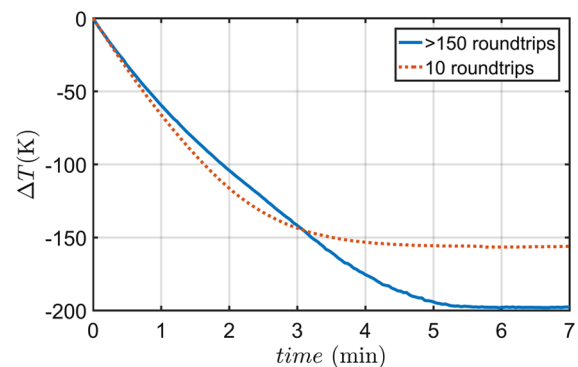


**Fig. 7** Comparing cooling results with 10 passes (red) and an astigmatic Herriott cell with more than 150 passes (blue).

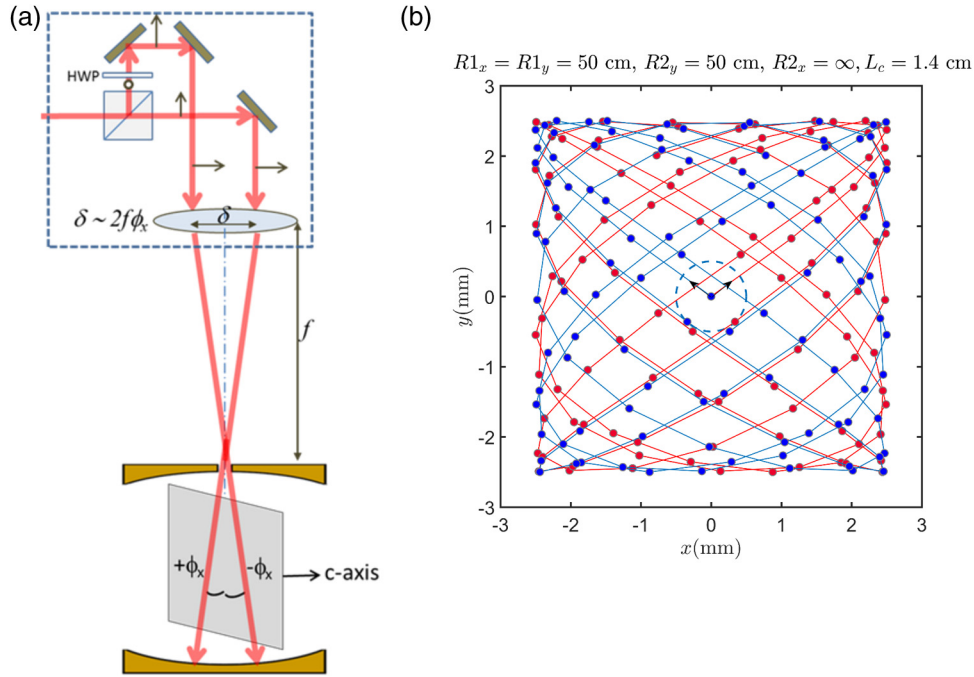


**Fig. 8** (a) Schematic for two beam pumping and (b) beam pattern on the mirror after 100 roundtrips.

$$S_{\text{DLT}}(T, T_0) = \int_{\lambda_1}^{\lambda_2} |\Delta S(\lambda, T)| d\lambda. \quad (6)$$

Temperature of the crystal is then determined by comparing this value to values calculated during a calibration process performed in a closed-cycle Helium cryostat from 70 to 300 K. The cooling results are shown in Fig. 7. Increasing the number of passes has improved the cooling almost by 50 K (details of these experiments are in preparation for publication).

While it is difficult to know exactly how many effective passes the sample has experienced at its lowest temperature point ( $\approx 90$  K), this preliminary experiment simply validates the utility of such astigmatic nonresonant cavities for maximizing the absorption while utilizing most of the crystal volume.

This further provides the advantage of allowing much higher incident powers without concerns of absorption saturation.

Finally, we consider the case involving high-power fiber lasers with unpolarized output. Linear polarization inside the cavity is still highly desired for mitigating Fresnel losses (Brewster condition) and maximizing absorption ( $E \parallel c$  for YLF crystal). We propose the approach shown in Fig. 8(a), where the unpolarized laser beam is divided into two p-polarized beams that are launched into the Herriott cell at angles of  $(\Phi_x, \Phi_y)$  and  $(-\Phi_x, \Phi_y)$ , respectively. The calculated corresponding pattern (beam locations) from both beams on mirror 1 using the same cavity parameters as in Fig. 4 is shown in Fig. 8(b). Note that the second beam can be launched alternatively at angle coordinates of  $(-\Phi_x, -\Phi_y)$  or  $(\Phi_x, -\Phi_y)$  with similar effect.

In conclusion, we have analyzed an astigmatic Herriott cell used in solid-state optical refrigeration. Such a cell

has enabled us to utilize the entire available laser power to cool to lower temperatures in a shorter time. Additionally, it potentially enables us to use unpolarized high-power lasers, and to achieve much higher cooling power for practical applications.

### Acknowledgments

The authors would like to acknowledge the support by AFOSR Grant FA9550-15-1-0241 and DARPA STTR Program. We also thank Professor Mauro Tonelli's group from University of Pisa, Italy, for providing the YLF crystal and Dr. Richard Epstein and Bernardo Farfan from Thermo-Dynamic Films (TDF) LLC for useful discussions.

### References

1. M. Sheik-Bahae and R. I. Epstein, "Optical refrigeration," *Nat. Photonics* **1**(12), 693–699 (2007).
2. M. Sheik-Bahae and R. I. Epstein, "Laser cooling of solids," *Laser Photonics Rev.* **3**(1–2), 67–84 (2009).
3. D. V. Seletskiy, M. P. Hasselbeck, and M. Sheik-Bahae, "Resonant cavity-enhanced absorption for optical refrigeration," *Appl. Phys. Lett.* **96**(18), 181106 (2010).
4. B. Heeg et al., "Experimental demonstration of intracavity solid-state laser cooling of  $\text{Yb}^{3+}$ :  $\text{ZrF}_4 - \text{BaF}_2 - \text{LaF}_3 - \text{AlF}_3 - \text{NaF}$  glass," *Phys. Rev. A* **70**(2), 021401 (2004).
5. M. Ghasemkhani et al., "Intra-cavity cryogenic optical refrigeration using high power vertical external-cavity surface-emitting lasers (VECSELs)," *Opt. Express* **22**(13), 16232–16240 (2014).
6. D. R. Herriott and H. J. Schulte, "Folded optical delay lines," *Appl. Opt.* **4**(8), 883 (1965).
7. J. B. McManus, P. L. Kebabian, and M. S. Zahniser, "Astigmatic mirror multipass absorption cells for long-path-length spectroscopy," *Appl. Opt.* **34**(18), 3336 (1995).
8. S. D. Melgaard et al., "Solid-state optical refrigeration to sub-100 Kelvin regime," *Sci. Rep.* **6**, 20380 (2016).
9. W. Patterson et al., "Differential luminescence thermometry in laser cooling of solids," *Proc. SPIE* **6461**, 64610B (2007).

Biographies for the authors are not available.